Proceedings of the 2002 IEEE
International Conference on Robotics & Automation
Washington, DC • May 2002

On-Line Terrain Parameter Estimation for Planetary Rovers

Karl Iagnemma *Hassan Shibly Steven Dubowsky

Field and Space Robotics Laboratory
Department of Mechanical Engineering
Massachusetts Institute of Technology
Cambridge, MA, 02215 U.S.A.

*Department of Mechanical Engineering, Bir-Zeit University
Palestinian Territories

Abstract

Future planetary exploration missions will require rovers to traverse very rough terrain with limited human supervision. Wheel-terrain interaction plays a critical role in rough-terrain mobility. In this paper an on-line estimation method that identifies key terrain parameters using on-board rover sensors is presented. These parameters can be used for accurate traversability prediction or in a traction control algorithm. These parameters are also valuable indicators of planetary surface soil composition. Simulation and experimental results show that the terrain estimation algorithm can accurately and efficiently identify key terrain parameters for loose sand.

1.0 Introduction and Related Work

Future planetary exploration missions will require rovers to perform challenging mobility tasks in rough terrain [5, 14, 16]. Proposed future mission objectives include traversal of several kilometers with a high degree of autonomy. To accomplish these objectives, future control and planning methods must consider the physical characteristics of the rover and its environment, to fully utilize the rover's capabilities.

Wheel-terrain interaction has been shown to play a critical role in rough-terrain mobility [1, 2]. For example, a vehicle traversing loose sand has very different mobility characteristics than one traversing firm clay. For planetary rovers, it is desirable to estimate terrain parameters on-line, since on-line estimation would allow a rover to accurately predict the traversability of neighboring terrain regions. Terrain parameter estimation would also allow a rover to adapt its control and planning strategy to a given terrain [7]. Off-line (i.e. Earth-based) estimation could be performed, but the associated communication time delays are extensive. Finally, on-line terrain estimation is desirable for enhancing our understanding of planetary surface composition.

Many researchers have studied methods for identifying key wheel-terrain interaction model parameters [12, 15]. Generally, these methods involve off-line estimation using costly, dedicated testing equipment. Terrain parameter estimation for a legged system has been documented in [3]. This approach uses an embedded three-axis force sensor, which most planetary rovers are not equipped with. Terrain parameter estimation for tracked vehicles has been proposed in [3]. This approach assumes a highly simplified "force coefficient" model of track-terrain interaction, which is not valid in deformable rough terrain.

Parameter estimation of Martian soil has been performed by the Viking landers and the Sojourner rover [10, 11]. The Viking landers used manipulator arms to conduct trenching experiments. The Sojourner rover used the rover wheel as a bevameter-type device to identify soil cohesion and internal friction angle. Both missions used visual cues and off-line analysis techniques to compute soil parameters.

In this paper, a method for on-line estimation of terrain cohesion and internal friction angle using on-board rover sensors is presented. The algorithm estimates parameters of the terrain the rover is currently traversing. The algorithm relies on a simplified form of classical terramechanics equations, and uses a linear-least squares estimator to compute terrain parameters in real time. The method is computationally efficient, and is thus suitable for implementation on a rover with limited on-board computational resources. Simulation and experimental results show that the terrain estimation algorithm can accurately and efficiently identify key terrain parameters for loose sand.

2.0 Terrain Parameter Identification

The purpose of terrain parameter identification is to estimate key terrain parameters on-line, using on-board rover sensors. Two key terrain parameters are the cohesion, c, and internal friction angle, ϕ. These parameters can be used to compute the terrain shear

strength, and thus give an estimate of the rover traversability, from Coulomb's equation:

$$\tau_{max} = (c + \sigma_{max} \tan\phi) \quad (1)$$

where σ is the normal stress acting on the terrain region. Here, the case of a smooth rigid wheel traveling through deformable terrain is considered, since this is the expected condition for planetary exploration vehicles. Note, however, that this case is common in terrestrial vehicles, since a pneumatic tire can be considered rigid if its inflation pressure is high compared to the terrain stiffness [1].

To estimate terrain physical parameters, equations relating the parameters of interest to physically measurable quantities must be developed. A free-body diagram of a driven rigid wheel traveling through deformable terrain is shown in Figure 1. A vertical load W and a horizontal force DP are applied to the wheel by the vehicle suspension. A torque T is applied at the wheel rotation axis by an actuator. The wheel has angular velocity ω, and the wheel center possesses a linear velocity, V. The angle from the vertical at which the wheel first makes contact with the terrain is denoted θ_1. The angle from the vertical at which the wheel loses contact with the terrain is denoted θ_2. Thus, the entire angular wheel-terrain contact region is defined by $\theta_1+\theta_2$.

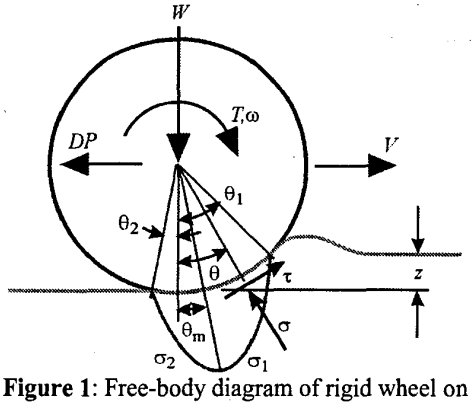

Figure 1: Free-body diagram of rigid wheel on deformable terrain

A stress region is created at the wheel-terrain interface, as indicated by the regions σ_1 and σ_2. At a given point on the interface, the stress can be decomposed into a component acting normal to the wheel at the wheel-terrain contact point, σ, and a component acting parallel to the wheel at the wheel-terrain contact point, τ. The angle from the vertical at which the maximum stress occurs is denoted θ_m.

In the following analysis it is assumed that the following quantities are known: the vertical load W, torque T, sinkage z, wheel angular speed ω, and wheel linear speed V. The vertical load W can be computed from a quasi-static analysis of the rover, with knowledge of the mass distribution. Static analysis is valid due to the low speeds of these vehicles (i.e. on the order of 10 cm/sec) [16]. The torque T can be estimated with reasonable accuracy from the current input to the wheel motor. The sinkage z can be computed from kinematic analysis of the rover suspension or via fused vision-odometry techniques [8, 17]. The wheel angular speed ω can be measured with a tachometer. The wheel linear speed V can be computed using IMU measurements, or vision-based scene analysis techniques [6]. Thus, all required inputs can be measured or estimated with on-board rover sensors.

Force balance equations are written for the system in Figure 1, as:

$$W = rb\left(\int_{\theta 1}^{\theta_2} \sigma(\theta)\cos\theta \cdot d\theta + \int_{\theta_1}^{\theta_2} \tau(\theta)\sin\theta \cdot d\theta\right) \quad (2)$$

$$DP = rb\left(\int_{\theta 1}^{\theta_2} \tau(\theta)\cos\theta \cdot d\theta - \int_{\theta_1}^{\theta_2} \sigma(\theta)\sin\theta \cdot d\theta\right) \quad (3)$$

$$T = r^2 b \int_{\theta_1}^{\theta_2} \tau(\theta) \cdot d\theta \quad (4)$$

The shear stress is described as:

$$\tau(\theta) = (c + \sigma(\theta)\tan\phi)\left(1 - e^{-\frac{r}{k}[\theta_1 - \theta - (1-i)(\sin\theta_1 - \sin\theta)]}\right) \quad (5)$$

where k is the shear deformation modulus, r is the wheel radius, and i is the wheel slip, defined as $i = 1 - (V/r\omega)$ [13, 18].

The normal stress at the wheel-terrain interface is given by:

$$\sigma(z) = (k_1 + k_2 b)\left(z/b\right)^n \quad (6)$$

where b is the wheel width, k_1 and k_2 are constants, and n is the sinkage coefficient [1]. An expression for the normal stress as a function of the wheel angular location θ is written by expressing the sinkage as a function of the angular location θ:

$$z(\theta) = r(\cos\theta - \cos\theta_1) \quad (7)$$

Substituting Equation (7) into Equation (6) yields expressions for the normal stress distribution along the wheel-terrain interface, as:

$$\sigma_1(\theta) = (k_1 + k_2 b)\left(r/b\right)^n (\cos\theta - \cos\theta_1)^n \quad (8)$$

$$\sigma_2(\theta) = (k_1 + k_2 b)\left(r/b\right)^n \left(\cos\left(\theta_1 - \frac{\theta}{\theta_m}(\theta_1 - \theta_m)\right) - \cos\theta_1\right)^n \quad (9)$$

Analytical expressions for the force balance equations (Equations (2-4)) are required to estimate the cohesion and internal friction angle. However, Equations (2-4) are not amenable to symbolic manipulation, due to their complexity. This complexity motivates the use of an approximate form of the stress equations.

2.1 Equation Simplification

Figure 2 is a plot of the shear and normal stress distributions (as defined by Equations (5) and (8-9), respectively) around the rim of a driven rigid wheel on deformable terrain for a range of slip, i, and sinkage coefficient, n. Note that although numerous parameters influence the shape of the stress distribution curves, n and i dominate, and are thus the primary parameters of interest.

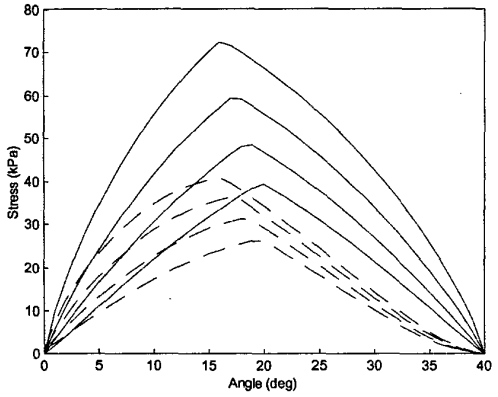

Figure 2: Normal stress (solid) and shear stress (dashed) distribution for varying slip and sinkage

The shear and normal stress distribution curves are approximately triangular for a wide range of parameters. Based on this observation, a linear approximation of the shear and normal stress distribution equations can be written as:

$$\sigma_1(\theta) = \frac{\theta_1 - \theta}{\theta_1 - \theta_m}\sigma_m \tag{10}$$

$$\sigma_2(\theta) = \frac{\theta}{\theta_m}\sigma_m \tag{11}$$

$$\tau_1(\theta) = \frac{\theta_1 - \theta}{\theta_1 - \theta_m}\tau_m \tag{12}$$

$$\tau_2(\theta) = \frac{\theta}{\theta_m}\tau_m \tag{13}$$

where σ_m and τ_m are the maximum values of the normal and shear stress, respectively.

Simulations were conducted to compare the linear approximations (Equations (10-13)) to the original nonlinear equations (Equations (5, 8-9)). Approximately 60,000 simulations were conducted in the following parameter space: $20.0 < \theta_1$ (deg) < 60.0, $0.6 < n < 1.2$, $20.0 < \phi$ (deg) < 40.0, $0.0 < c$ (kPa) < 3.0, $0.0 < k_1$ (kPa) < 140.0, $520.0 < k_2$ (kN/m^3) < 680.0, $0.005 < k$ (m) < 0.04, $0.0 < i < 1.0$. The simulated wheel radius r was 0.25 m, and the width b was 0.2 m. These parameter ranges are reasonable for a small planetary exploration rovers traveling on deformable terrain.

An average difference of 9.34% was found between the approximate and actual normal stress distribution equations, and 12.15% between the approximate and actual shear stress distribution equations. Thus, the linear approximations were considered sufficiently accurate representations of the true nonlinear functions.

Simplified forms of the force balance equations can now be written by combining Equations (2-4) and Equations (10-13), as:

$$W = rb\left(\begin{array}{l}\int_0^{\theta_m}\sigma_2(\theta)\cos\theta\cdot d\theta + \int_{\theta_m}^{\theta_1}\sigma_1(\theta)\cos\theta\cdot d\theta \\ +\int_0^{\theta_m}\tau_2(\theta)\sin\theta\cdot d\theta + \int_{\theta_m}^{\theta_1}\tau_1(\theta)\sin\theta\cdot d\theta\end{array}\right) \tag{14}$$

$$DP = rb\left(\begin{array}{l}\int_0^{\theta_m}\tau_2(\theta)\cos\theta\cdot d\theta + \int_{\theta_m}^{\theta_1}\tau_1(\theta)\cos\theta\cdot d\theta \\ -\int_0^{\theta_m}\sigma_2(\theta)\sin\theta\cdot d\theta - \int_{\theta_m}^{\theta_1}\sigma_1(\theta)\sin\theta\cdot d\theta\end{array}\right) \tag{15}$$

$$T = r^2 b\left(\int_0^{\theta_m}\tau_2(\theta)\cdot d\theta + \int_{\theta_m}^{\theta_1}\tau_1(\theta)\cdot d\theta\right) \tag{16}$$

Evaluation of Equations (14) and (16) leads to the following expressions for the normal load and torque:

$$W = \frac{rb}{\theta_m(\theta_1 - \theta_m)}\left[\begin{array}{l}\sigma_m(\theta_1\cos\theta_m - \theta_m\cos\theta_1 - \theta_1 + \theta_m) \\ +\tau_m(\theta_1\sin\theta_m - \theta_m\sin\theta_1)\end{array}\right] \tag{17}$$

$$T = \frac{1}{2}r^2 b\tau_m\theta_1 \tag{18}$$

Two assumptions are made in solving Equations (17) and (18). The first is that the location of the maximum shear and normal stress occur at the same location θ_m. Analysis and simulation has shown that this assumption is reasonable for a wide range of soil values. With this assumption, an additional relation can be written, based on Equation (5):

$$\tau_m = (c+\sigma_m \tan\phi)\left(1-e^{-\frac{r}{k}[\theta_1-\theta_m-(1-i)(\sin\theta_1-\sin\theta_m)]}\right) \quad (19)$$

The second assumption is that the angular location of maximum stress, θ_m, occurs midway between θ_1 and θ_2, i.e. $\theta_m = (\theta_1+\theta_2)/2$. Analysis and simulation has shown that this assumption is reasonable for a wide range of soils with low to moderate slip ratios.

The system of Equations (17-19) can be combined into a single equation relating the cohesion and internal friction angle (with $\theta_2 = 0$), as:

$$c = \frac{\left(\left(4T\sin(\theta_1)+W\theta_1^2 r-8T\sin(\frac{\theta_1}{2})\right)\tan(\phi)+\left(4T\cos(\theta_1)-8T\cos(\frac{\theta_1}{2})+4T\right)\Big/(1-A_1)\right)}{2r^2 w\theta_1\left(\cos(\theta_1)-2\cos(\frac{\theta_1}{2})+1\right)} \quad (20)$$

where $A_1 = e^{-\frac{r}{k}\left(\frac{\theta_1}{2}+(1-i)\left(-\sin(\theta_1)+\sin(\frac{\theta_1}{2})\right)\right)}$.

Equations (20) is a single equation in two unknowns. During the parameter estimation process, sensor data is recorded at each sampling point j. Thus, for a rover moving at low speed with a reasonable sampling rate (i.e. several hertz), numerous data points can be collected within a small terrain region. Equation (20) can then be written j times, and solved in a least-squares fashion, as:

$$\mathbf{K}_1 = \mathbf{K}_2\begin{bmatrix} c \\ \tan\phi \end{bmatrix} \quad (21)$$

$$\begin{bmatrix} c \\ \tan\phi \end{bmatrix} = \left(\mathbf{K}_2^T\mathbf{K}_2\right)^{-1}\mathbf{K}_2^T\mathbf{K}_1 \quad (22)$$

with $\mathbf{K}_1 = \begin{bmatrix} K_{11} & K_{12} & \cdots & K_{1j} \end{bmatrix}^T$, $\mathbf{K}_2 = \begin{bmatrix} \mathbf{K}_{21} & \mathbf{K}_{22} & \cdots & \mathbf{K}_{2j} \end{bmatrix}^T$, and

$$K_1 = \left(4T\cos(\theta_1)-8T\cos(\frac{\theta_1}{2})+4T\right)\Big/(1-A_1)$$

$$\mathbf{K}_2 = \begin{bmatrix} 2r^2 w\theta_1\left(\cos(\theta_1)-2\cos(\frac{\theta_1}{2})+1\right) \\ -\left(4T\sin(\theta_1)+W\theta_1^2 r-8T\sin(\frac{\theta_1}{2})\right) \end{bmatrix}^T$$

All quantities in Equation (22) can be sensed except the shear deformation modulus k. However, the estimation process exhibits low sensitivity to error in k, and thus k is chosen as a representative value for deformable terrain.

3.0 Simulation Results

Simulations were conducted in Matlab of a single driven wheel traveling through deformable terrain. The purpose of the simulation was to examine the accuracy of the parameter estimation algorithm in the presence of noisy and uncertain inputs.

The wheel was commanded to travel at approximately 5 cm/sec. The simulated sensor inputs W, T, z, and i were corrupted with white noise of a magnitude equivalent to 10% of their maximum value. The simulated sampling rate was 10 Hz. The shear deformation modulus k was assumed to be 300% of its actual value.

The following parameter set was used: $r = 0.5$ m, $w = 0.3$ m, $k = 0.005$ m, $k_1 = 20.0$ kPa, $k_2 = 600$ kN/m3, $n = 0.9$. The cohesion and internal friction angle were $c = 1.0$ kPa, $\phi = 30.0$. These parameters were chosen for their similarity to terrain a planetary exploration rover might encounter [4, 10].

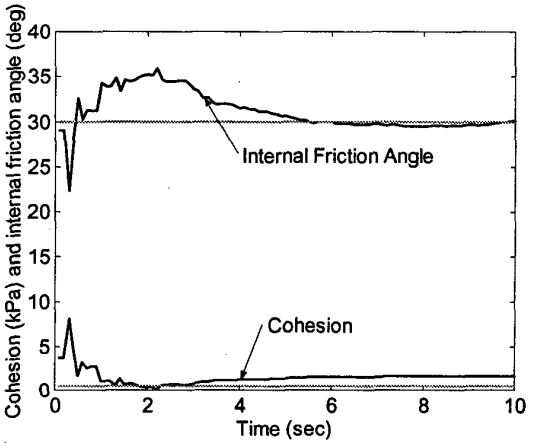

Figure 3: Simulated comparison of estimated cohesion (black) and internal friction angle (black) estimation to true values (gray)

A representative result is shown in Figure 3. It can be seen that the estimated parameters rapidly approach their true values. Small differences remains, due to the simplifying assumptions in the estimation process. However, it can be seen that the estimation algorithm produces accurate results. The computational load for the algorithm is approximately 2-3 msec per estimation cycle for unoptimized Matlab code.

The simplifying assumptions also allow prediction of the drawbar pull (Equation (15)) using only sensed inputs. The drawbar pull is a measure of the net forward force created by the wheel, and is thus an important part of traversability prediction. Figure 4 shows a comparison of the actual and predicted drawbar pull for the simulation run described above. The predicted drawbar pull is very close to the actual value.

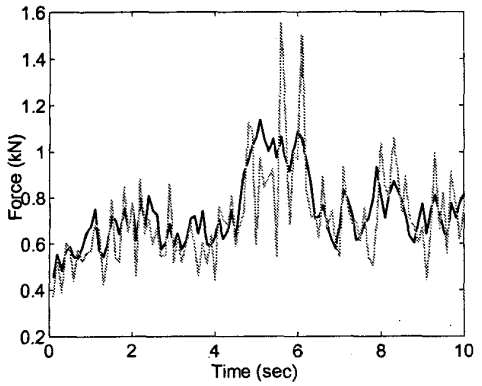

Figure 4: Actual (black) and predicted (gray) drawbar pull

4.0 Experimental Results

Experiments were performed on the Field and Space Robotics Laboratory terrain characterization testbed, shown in Figure 5. The testbed consists of a driven rigid wheel mounted on an undriven vertical axis. The wheel assembly is mounted to a driven horizontal carriage. By driving the wheel and carriage at different rates, variable slip ratios can be imposed. The vertical wheel load can be changed by adding weight to the vertical axis.

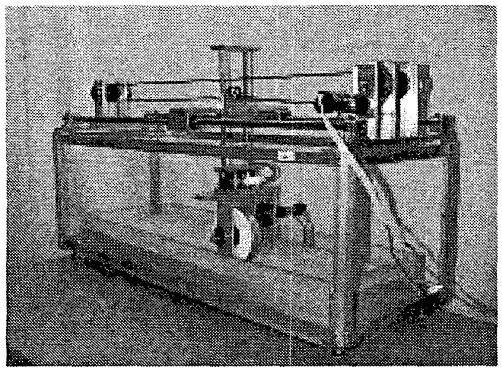

Figure 5: Field and Space Robotics Laboratory terrain characterization testbed

The testbed is instrumented with encoders to measure angular velocities of both the wheel and the carriage pulley. The carriage linear velocity is computed from the carriage pulley angular velocity. The vertical wheel sinkage is measured with a linear potentiometer. The current input to the wheel is estimated by measuring the voltage across a current-sense resistor. The six-component wrench between the wheel and carriage is measured with an AMTI six-axis force/torque sensor. The force sensor allows measurement of the normal load W and drawbar pull DP. The estimation algorithm is run on an Intel 486 66 Mhz processor at a rate of 250 Hz.

The wheel diameter and width are 14.6 and 6.0 cm., respectively. The wheel maximum angular velocity is 1.1 rad/sec. This results in a maximum linear velocity of 8.0 cm/sec, which is identical to the maximum carriage velocity. The wheel size and speed were chosen to be similar to current and projected planetary rovers.

Terrain parameter identification experiments were run in sand. Results of a representative experiment are shown in Figure 6. The estimation algorithm gives parameter estimates for c and ϕ in the range of –3.1-2.2 kPa and 26°-43°, respectively. (Note that estimated negative values for cohesion are not physically meaningful.) Published data for c and ϕ for loose sand falls in a range between 0-1.0 kPa and 25°-32°, respectively [1]. Experiments to characterize loose sand with a bevameter has confirmed these parameter ranges [8]. Thus, the estimation algorithm produces reasonable results on an experimental system. Error sources are sensor noise, and soil inhomogeneities caused by non-uniform soil mixing.

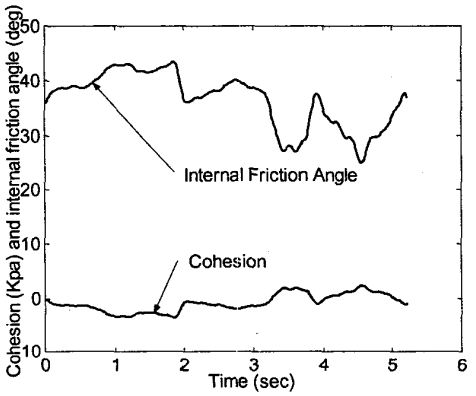

Figure 6: Experimental results of cohesion and internal friction angle estimation

Figure 7 shows a comparison of the measured and predicted drawbar pull for the wheel system. Again, the results are reasonably close.

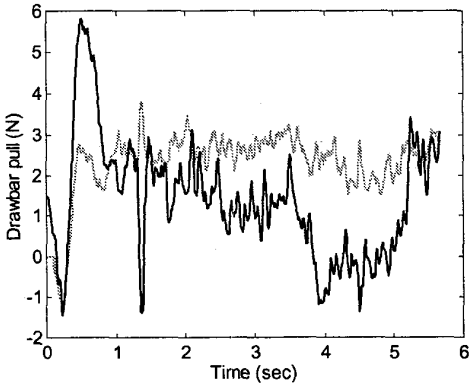

Figure 7: Measured (black) and predicted (gray) DP

5.0 Summary and Future Work

An on-line terrain parameter estimation algorithm has been presented. The estimation method is based on simplified forms of classical terramechanics equations. The simplified equations are solved for the cohesion and internal friction angle. A linear least-squares estimator is formulated to estimate the cohesion and internal friction angle in real time. Simulation and experimental results show that the estimation method can estimate terrain parameters with good accuracy in the presence of noise, using limited computational resources, making the method potentially suitable for on-line implementation. Experimental results with a terrain characterization testbed confirm these results for beach sand.

Future work in this area will focus on improving the estimation method's robustness to sensor noise and error. Integration of the parameter estimation method into a comprehensive terrain typing algorithm will also be studied.

Acknowledgments

This work is supported by the NASA Jet Propulsion Laboratory. The authors would like to acknowledge the support and assistance of Dr. Paul Schenker and Dr. Samad Hayati at JPL.

References

[1] Bekker, G., *Theory of Land Locomotion,* University of Michigan Press, 1956

[2] Bekker, G., *Introduction to Terrain-Vehicle Systems,* University of Michigan Press, 1969

[3] Caurin, G., and Tschichold-Gurman, N., "The Development of a Robot-Terrain Interaction System for Walking Machines," *IEEE International Conference on Robotics and Automation*, Volume 2, pp. 1013-1018, 1994

[4] Haldemann, A., "Mars Soils White Paper v. 1.2," http:// mvacs.ess.ucla.edu /mvacs/ envi/ soil/wht-ppr. html

[5] Hayati, S., Volpe, R., Backes, P., Balaram, J., and Welch, W., "Microrover Research for Exploration of Mars," *AIAA Forum on Advanced Developments in Space Robotics,* 1996

[6] Hogg, R., Rankin, A., McHenry, M., Helmick, D., Bergh, C., Roumeliotis, S., Matthies, L., "Sensors and Algorithms for Small Robot Leader/Follower Behavior," *Proceedings of the 15th SPIE AeroSense Symposium,* 2001

[7] Iagnemma, K., and Dubowsky, S., "Mobile Robot Rough-Terrain Control (RTC) for Planetary Exploration," Proceedings *of the 26th ASME Biennial Mechanisms and Robotics Conference, DETC 2000,* 2000

[8] Iagnemma, K., *Rough-Terrain Mobile Robot Planning and Control, with Application to Planetary Exploration,* Ph.D. Thesis, Massachusetts Institute of Technology, Cambridge, MA, 2001

[9] Le, A., Rye, D., and Durrant-Whyte, H., "Estimation of Track-Soil Interactions for Autonomous Tracked Vehicles," *Proc. of the IEEE International Conf. on Robotics and Automation,* pp. 1388-1393, 1997

[10] Matijevic, J., *et al.*, "Characterization of Martian Surface Deposits by the Mars Pathfinder Rover, Sojourner," *Science*, Volume 278, Number 5, pp. 1765-1768, 1997

[11] Moore, H., Hutton, R., Scott, R., Spitzer, C., and Shorthill, R., "Surface Materials of the Viking Landing Sites, Mars," *Journal of Geophysical Research,* Vol. 82, No. 28, 1977

[12] Nohse, Y., Hashuguchi, K., Ueno, M., Shikanai, T., Izumi, H., and Koyama, F., "A Measurement of Basic Mechanical Quantities of Off-The-Road Traveling Performance," *Journal of Terramechanics*, Volume 28, Number 4, pp. 359-371, 1991

[13] Onafeko, O., and Reece, A., "Soil Stresses and Deformation Beneath Rigid Wheels", *Journal of Terramechanics*, Vol. 4, Number 1, pp. 59-80, 1967

[14] Schenker, P., *et al.*, "Lightweight Rovers for Mars Science Exploration and Sample Return," *Proceedings of SPIE XVI Intelligent Robots and Computer Vision Conference*, Volume 3208, pp. 24-36, 1997

[15] Shmulevich, I., Ronai, D., and Wolf, D., "A New Field Single Wheel Tester," *Journal of Terramechanics,* Volume 33, Number 3, pp. 133-141, 1996

[16] Weisbin, C., Rodriguez, G., Schenker, P., Das, H., Hayati, S., Baumgartner, E., Maimone, M., Nesnas, I., and Volpe, R., "Autonomous Rover Technology for Mars Sample Return," *1999 International Symposium on Artificial Intelligence, Robotics and Automation in Space (i-SAIRAS '99)*, 1999

[17] Wilcox, B., "Non-Geometric Hazard Detection for a Mars Microrover," *Proceedings of the AIAA Conference on Intelligent Robotics in Field,Factory, Service, and Space,* Volume 2, 1994

[18] Wong, J., and Reece, A, "Prediction of Rigid Wheels Performance Based on Analysis of Soil-Wheel Stresses, Part I," *Journal of Terramechanics,* Volume 4, Number 1, pp. 81-98, 1967